International Journal of Heat and Mass Transfer 53 (2010) 4552–4566

Contents lists available at ScienceDirect

International Journal of Heat and Mass Transfer

journal homepage: www.elsevier.com/locate/ijhmt

Analytical heat diffusion models for heat sinks with circular micro-channels

Sung-Min Kim, Issam Mudawar *

Boiling and Two-Phase Flow Laboratory (BTPFL) and Purdue University International Electronic Cooling Alliance (PUIECA), Mechanical Engineering Building, 585 Purdue Mall, West Lafayette, IN 47907-2088, USA

ARTICLE INFO

Article history:
Received 23 December 2009
Received in revised form 10 June 2010
Accepted 10 June 2010
Available online 16 July 2010

Keywords:
Micro-channel
Heat diffusion
Analytical model

ABSTRACT

This study explores the prediction of temperature distribution in a heat sink containing an array of circular micro-channels, which is found mostly in electronic cooling applications. The analytical heat diffusion models for most common micro-channel shapes are based on one-dimensional fin models with varying degrees of complexity. Because of a singularity in the governing one-dimensional heat diffusion equation for a fin with circular profile, no exact solution is possible for the circular heat sink geometry. In this paper, an alternative analytical power series solution technique is presented in which the differential equation is recast in polynomial form. Predictions of the power series solution are validated for different channel diameters and spacings and both one-sided and two-sided heating conditions using one-dimensional and two-dimensional numerical simulations. Overall, maximum percent differences in temperature and heat transfer rate between the analytical and two-dimensional numerical results of 0.23% and 1.33%, respectively, prove that the present analytical models are very accurate and effective tools for the design and thermal resistance prediction of micro-channel heat sinks found in electronic cooling applications.

1. Introduction

Interest in developing compact, high-flux thermal management solutions for many pressing electronic cooling problems is behind the many recent studies concerning micro-channel heat sinks [e.g., [1–4]]. These devices feature compactness, small coolant inventory, and high power dissipation to volume ratio, especially when the coolant is allowed to undergo phase change along the micro-channels. Because of the relative simplicity of fabricating rectangular micro-channels, the vast majority of electronic cooling studies since the early 1980s involve rectangular cross-sections. However, an increasing number of single-phase and two-phase heat transfer studies are focusing on heat sinks having non-rectangular cross-sections such as triangular [5,6], trapezoidal [7–10], and circular [11,12], citing thermal benefits to these cross-sections related to heat diffusion effects or bubble nucleation in sharp corners.

Heat sinks with circular cross-sections have been around before 1980 and involve applications other than electronic cooling. For example, flow boiling in circular micro-channels has been the subject of intense study since the mid-1970s at the Massachusetts Institute of Technology Energy Laboratory for cooling of electrodes in magnetohydrodynamic energy converters and turbine blades [13]. In the mid-1990s, Bowers and Mudawar [14] proposed the first use of heat sinks with circular micro-channels for electronic cooling, and provided the first systematic methodology for thermal design of micro-channel heat sinks undergoing phase change. Mudawar and Bowers [15] and Hall and Mudawar [16] later showed that highly subcooled and high mass velocity flow boiling of water in small diameter tubes could safely dissipate heat fluxes as high as 27,000 W/cm^2.

Fig. 1 shows schematic diagrams of two types of heat sinks containing linear arrays of circular micro-channels. The first, Fig. 1(a), is subjected to one-sided heating and the second, Fig. 1(b), symmetrical two-sided heating. In an electronic cooling application, the base heat flux, q''_{base}, and the base temperature, T_{base}, in Fig. 1(a) correspond to the device heat flux and device temperature, respectively, which are known. A major unknown is the heat transfer coefficient, which can be determined from the relation $h = q''_{eff}/(T_w - T_f)$, where q''_{eff}, T_w, and T_f are the average heat flux along the micro-channel wall, the average channel wall temperature, and the bulk fluid temperature, respectively. While q''_{eff} can be easily determined from a simple energy balance for the entire heat sink, a method is needed to determine T_w in order to calculate h. This is where an analytical heat diffusion model of the heat sink is desired, which is the primary goal of this study.

This study is a follow-up to a recent study by the present authors concerning the prediction of temperature distribution in heat sinks having micro-channels with rectangular, inverse-trapezoidal, triangular, trapezoidal, and diamond-shaped cross-sections [17]. Detailed analytical models for all these geometries were based on fin models with three basic profiles: rectangular,

* Corresponding author. Tel.: +1 765 494 5705; fax: +1 765 494 0539.
E-mail address: mudawar@ecn.purdue.edu (I. Mudawar).

0017-9310/$ - see front matter © 2010 Elsevier Ltd. All rights reserved.
doi:10.1016/j.ijheatmasstransfer.2010.06.038

Nomenclature

$a_0, a_1, \ldots$	coefficients in series
$A_0, A_1, \ldots$	coefficients in series
A_c	cross-sectional area of fin
A_{eff}	total wetted area of micro-channels
A_s	surface area of fin exposed to convection
b	fin length
Bi	Biot number, $h(W_s + D)/2k$
$c_0, c_1, \ldots$	coefficients in series
$C_0, C_1, \ldots$	coefficients in series
D	micro-channel diameter
h	heat transfer coefficient
H_b	distance from bottom of heat sink to bottom of micro-channel
H_c	distance from top of heat sink to top of micro-channel
k	thermal conductivity of heat sink solid
L	depth of heat sink
m	indices in series
N	number of micro-channels in heat sink
p	dimensionless fin parameter, $2\,bh/k$
$\hat{p}$	dimensionless fin parameter, hD/k
Q	heat transfer rate per unit length
q'	heat transfer rate per unit length
q''	heat flux
q''_{base}	heat flux based on base area of heat sink; device heat flux
q''_{eff}	heat flux based on heated perimeter of micro-channel
r	root in indical equation
s	indices in series
T	temperature
T_2	mean temperature defined in Fig. 3
T_{base}	temperature of heat sink base; device temperature
T_{fin}	mean temperature defined in Fig. 3
T_{tip}	mean temperature defined in Fig. 3
W_s	distance between micro-channels
$W_{s,e}$	width of endwall
x	coordinate
x'	coordinate
y	coordinate
X	coordinate
Y	coordinate
Z	denominator parameter
z'	parameter defined in Eq. (43)
Greek symbols	
δ_{fin}	fin thickness at base
θ	temperature difference
θ'	temperature difference
Subscripts	
1	lower quadrant surface of micro-channel
2	solid wall at $X = 0.5D$
2*a*	upper quadrant surface of micro-channel
A	analytical
base	heat sink base
f	bulk fluid
fin	fin base; solid wall at $X = 0$
N	numerical
tip	solid wall at $X = D$.

trapezoidal, and inverse-trapezoidal. The analytical results were compared to detailed two-dimensional numerical models of the same cross-sections for different micro-channel aspect ratios, fin spacings and Biot numbers. These comparisons proved the analytical models are very accurate tools for thermal resistance prediction of micro-channel heat sinks found in electronic cooling applications.

Because of a singularity in the governing one-dimensional heat diffusion equation for a fin with circular profile, no exact solution is possible for the circular heat sink geometry. Therefore, an alternative analytical power series solution technique is presented in the present paper in which the differential equation is recast in polynomial form. Solutions are presented for the two heating conditions illustrated in Fig. 1. To validate the analytical solutions, a parametric study of channel diameter, channel spacing, and Biot number is performed, and the analytical predictions are compared to one-dimensional and two-dimensional numerical solutions.

2. Analytical model for longitudinal fin with circular profile

2.1. General fin equation

Fig. 2 shows a schematic diagram of a longitudinal fin with a circular profile that is used to derive the diffusion models for the heat sinks illustrated in Fig. 1. The following conventional assumptions are made in the one-dimensional fin analysis [18,19]:

1. The heat conduction in the fin is steady and one-dimensional along the x-direction.
2. The fin material is homogeneous and isotropic.
3. The thermal conductivity of the fin is constant and uniform.
4. The heat exchange between the fin and the surrounding fluid is solely by convection along the fin surface.
5. There is no heat generation within the fin itself.
6. The heat transfer coefficient and the temperature of the surrounding fluid are constant and uniform.

Applying energy conservation to the differential element shown in Fig. 2, the governing second-order ordinary differential equation for one-dimensional steady-state temperature distribution can be derived as follows [20]

$$\frac{d^2T(x)}{dx^2} + \left(\frac{1}{A_c}\frac{dA_c(x)}{dx}\right)\frac{dT(x)}{dx} - \left(\frac{1}{A_c}\frac{h}{k}\frac{dA_s(x)}{dx}\right)(T(x) - T_f) = 0, \quad (1)$$

where A_c and A_s are the cross-sectional area and the surface area of the fin exposed to convection, respectively.

For a longitudinal fin with a circular profile, the following relations apply,

$$A_c = \delta_{fin} - 2\sqrt{b^2 - x^2}, \quad (2)$$

$$\frac{dA_c}{dx} = \frac{2x}{\sqrt{b^2 - x^2}}, \quad (3)$$

and $$\frac{dA_s}{dx} = 2\sqrt{1 + \left(\frac{dy}{dx}\right)^2} = \frac{2b}{\sqrt{b^2 - x^2}}. \quad (4)$$

Substituting Eqs. (2)–(4) into Eq. (1), yields

$$\frac{d^2\theta(x)}{dx^2} + \left(\frac{2x}{\delta_{fin}\sqrt{b^2 - x^2} - 2(b^2 - x^2)}\right)\frac{d\theta(x)}{dx} - \left(\frac{p}{\delta_{fin}\sqrt{b^2 - x^2} - 2(b^2 - x^2)}\right)\theta(x) = 0, \quad (5)$$

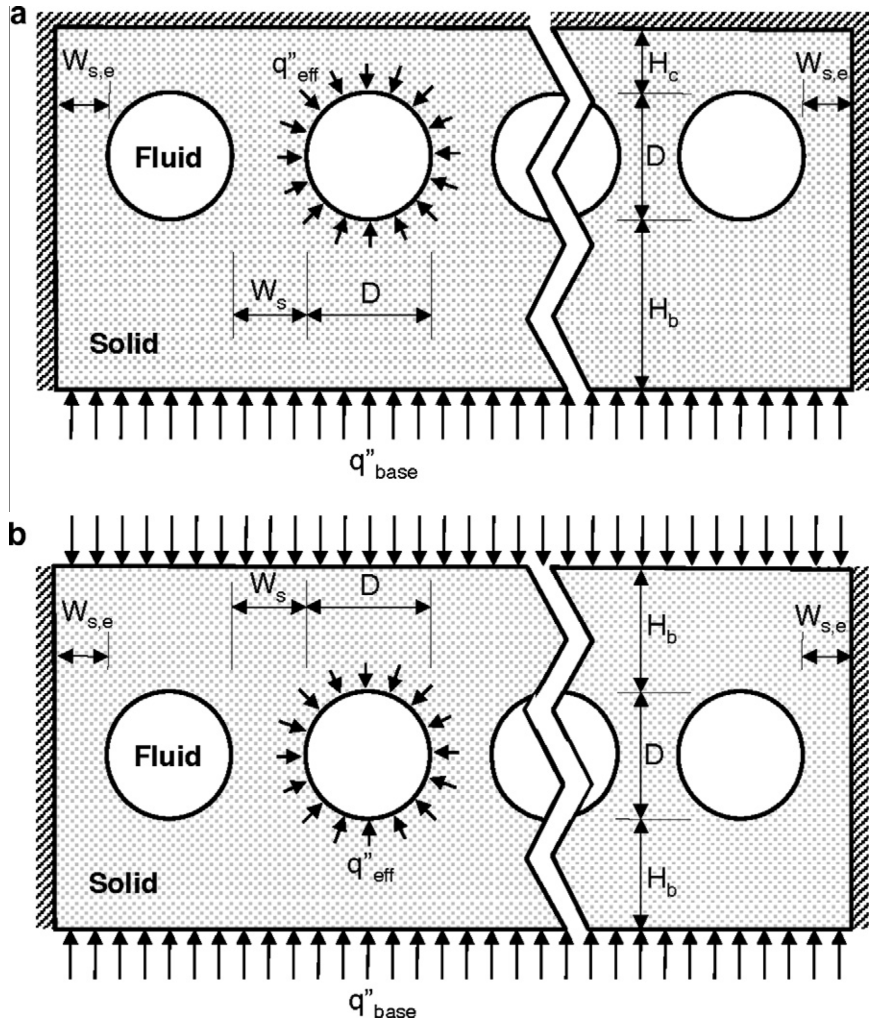

Fig. 1. Schematic diagrams of circular micro-channel heat sinks with (a) one-sided heating and (b) symmetrical two-sided heating.

where the temperature difference and the dimensionless fin parameter are defined as $\theta(x) = T(x) - T_f$ and

$$p = \frac{2bh}{k}. \tag{6}$$

Eq. (5) is a second-order ordinary differential equation with a singularity point at $x = b$, and, according to Polyanin and Zaitsev [21], has no exact solution.

2.2. New power series solution

In the present study, an alternative analytical power series solution technique is presented in which Eq. (5) is recast in polynomial form. To remove the square root terms in the denominator, a new term $z = \sqrt{b^2 - x^2}$ is introduced. Then

$$\frac{dz}{dx} = -\frac{x}{\sqrt{b^2 - x^2}}, \tag{7}$$

$$\frac{d\theta}{dx} = \frac{d\theta}{dz}\frac{dz}{dx} = -\frac{x}{\sqrt{b^2 - x^2}}\frac{d\theta}{dz}, \tag{8}$$

and $$\frac{d^2\theta}{dx^2} = \frac{d}{dx}\left(\frac{d\theta}{dx}\right) = \frac{-b^2}{(b^2 - x^2)\sqrt{b^2 - x^2}}\frac{d\theta}{dz} + \frac{x^2}{b^2 - x^2}\frac{d^2\theta}{dz^2}. \tag{9}$$

Substituting Eqs. (8) and (9) into Eq. (5) yields

$$\frac{d^2\theta(z)}{dz^2} + \left(\frac{2z^3 - b^2\delta_{fin}}{2z^4 - \delta_{fin}z^3 - 2b^2z^2 + \delta_{fin}b^2z}\right)\frac{d\theta(z)}{dz} - \left(\frac{pz}{2z^3 - \delta_{fin}z^2 - 2, b^2z + \delta_{fin}b^2}\right)\theta(z) = 0. \tag{10}$$

Eq. (10) can be presented in the following polynomial form

$$(2z^4 - \delta_{fin}z^3 - 2b^2z^2 + b^2\delta_{fin}z)\frac{d^2\theta(z)}{dz^2} + (2z^3 - b^2\delta_{fin})\frac{d\theta(z)}{dz} - pz^2\theta(z) = 0. \tag{11}$$

Assuming a solution in the form of a power series with unknown coefficients a_0, a_1, a_2,...

$$\theta(z) = \sum_{m=0}^{\infty} a_m z^{m+r} = a_0z^r + a_1z^{r+1} + a_2z^{r+2} + \cdots \tag{12}$$

Performing the first and second differentiation of Eq. (12) relative to z give, respectively,

$$\frac{d\theta}{dz} = \sum_{m=0}^{\infty}(m+r)a_m z^{m+r-1} = ra_0z^{r-1} + (r+1)a_1z^r + (r+2)a_2z^r + \cdots \tag{13}$$

and

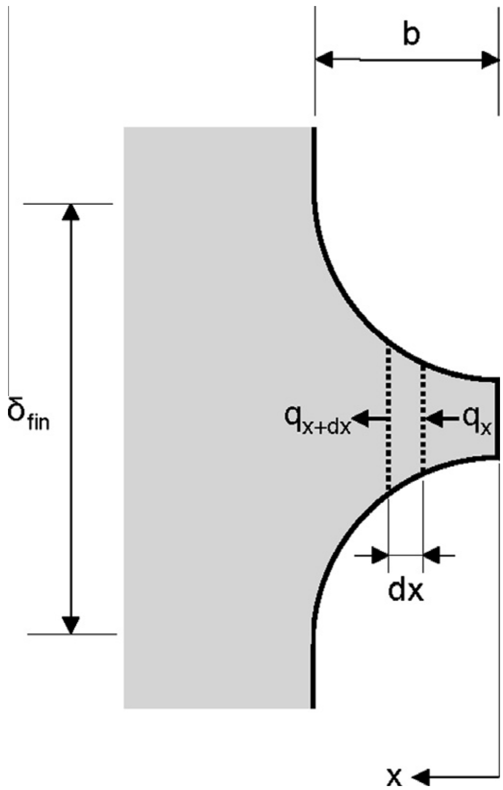

Fig. 2. Schematic diagram of longitudinal fin with circular profile.

$$\frac{d^2\theta}{dz^2} = \sum_{m=0}^{\infty}(m+r)(m+r-1)a_m z^{m+r-2}$$
$$= r(r-1)a_0 z^{r-2} + (r+1)r a_1 z^{r-1} + (r+2)(r+1)a_2 z^r + \cdots \tag{14}$$

Substituting Eqs. (13) and (14) into Eq. (11), and rearranging terms yields the following equation,

$$2\sum_{m=0}^{\infty}(m+r)(m+r-1)a_m z^{m+r+2} - \delta_{fin}\sum_{m=0}^{\infty}(m+r)(m+r-1)a_m z^{m+r+1}$$
$$-2b^2\sum_{m=0}^{\infty}(m+r)(m+r-1)a_m z^{m+r}$$
$$+b^2\delta_{fin}\sum_{m=0}^{\infty}(m+r)(m+r-1)a_m z^{m+r-1} + 2z^3\sum_{m=0}^{\infty}(m+r)a_m z^{m+r-1}$$
$$-b^2\delta_{fin}\sum_{m=0}^{\infty}(m+r)a_m z^{m+r-1} - pz^2\sum_{m=0}^{\infty}a_m z^{m+r} = 0. \tag{15}$$

Combining the series terms of Eq. (15) with the same power,

$$\sum_{m=0}^{\infty}[2(m+r)^2 - p]a_m z^{m+r+2} - \sum_{m=0}^{\infty}\delta_{fin}(m+r)(m+r-1)a_m z^{m+r+1}$$
$$-\sum_{m=0}^{\infty}2b^2(m+r)(m+r-1)a_m z^{m+r}$$
$$+\sum_{m=0}^{\infty}b^2\delta_{fin}(m+r)(m+r-2)a_m z^{m+r-1} = 0. \tag{16}$$

Eq. (16) can be modified to yield the same power, z^{s+r}, in all four series terms.

$$\sum_{s=2}^{\infty}[2(s+r-2)^2 - p]a_{s-2}z^{s+r} - \sum_{s=1}^{\infty}\delta_{fin}(s+r-1)(s+r-2)a_{s-1}z^{s+r}$$
$$-\sum_{s=0}^{\infty}2b^2(s+r)(s+r-1)a_s z^{s+r}$$
$$+\sum_{s=-1}^{\infty}b^2\delta_{fin}(s+r+1)(s+r-1)a_{s+1}z^{s+r} = 0. \tag{17}$$

The last three terms of Eq. (17) can be expressed individually as follows:

$$-\sum_{s=1}^{\infty}\delta_{fin}(s+r-1)(s+r-2)a_{s-1}z^{s+r}$$
$$= -\delta_{fin}r(r-1)a_0 z^{r+1} - \sum_{s=2}^{\infty}\delta_{fin}(s+r-1)(s+r-2)a_{s-1}z^{s+r}, \tag{18}$$

$$-\sum_{s=0}^{\infty}2b^2(s+r)(s+r-1)a_s z^{s+r} = -2b^2 r(r-1)a_0 z^r - 2b^2(r+1)r a_1 z^{r+1}$$
$$-\sum_{s=2}^{\infty}2b^2(s+r)(s+r-1)a_s z^{s+r}, \tag{19}$$

$$\sum_{s=-1}^{\infty}b^2\delta_{fin}(s+r+1)(s+r-1)a_{s+1}z^{s+r} = b^2\delta_{fin}r(r-2)a_0 z^{r-1}$$
$$+b^2\delta_{fin}(r+1)(r-1)a_1 z^r + b^2\delta_{fin}(r+2)r a_2 z^{r+1}$$
$$+\sum_{s=2}^{\infty}b^2\delta_{fin}(s+r+1)(s+r-1)a_{s+1}z^{s+r}. \tag{20}$$

Introducing Eqs. (18)–(20) into Eq. (17), gives

$$b^2\delta_b r(r-2)a_0 z^{r-1} + [b^2\delta_{fin}(r+1)(r-1)a_1 - 2b^2 r(r-1)a_0]z^r$$
$$+[b^2\delta_{fin}(r+2)r a_2 - 2b^2(r+1)r a_1 - \delta_{fin}r(r-1)a_0]z^{r+1}$$
$$+\sum_{s=2}^{\infty}\{[2(s+r-2)^2 - p]a_{s-2} - \delta_{fin}(s+r-1)(s+r-2)a_{s-1}$$
$$-2b^2(s+r)(s+r-1)a_s + b^2\delta_{fin}(s+r+1)(s+r-1)a_{s+1}\}z^{s+r} = 0. \tag{21}$$

To satisfy Eq. (21), all coefficients of z^{r-1}, z^r, z^{r+1} and z^{s+r} must be equal to zero. Assuming $a_0 \neq 0$, the first term in Eq. (21) yields

$$r(r-2) = 0. \tag{22}$$

This gives two values for r, $r_1 = 2$ and, $r_2 = 0$. Each value yields a series solution for $\theta(z)$, based on Eq. (12), whose coefficients a_m are determined by setting the coefficients of z^{r-1}, z^r, z^{r+1} and z^{s+r} in Eq. (21) equal to zero. For $r_1 = 2$, the coefficients of the series

$$\theta_1(z) = \sum_{m=0}^{\infty}a_m z^{m+2}, \tag{23}$$

are

$$a_1 = \frac{4}{3\delta_{fin}}a_0, \tag{24a}$$

$$a_2 = \frac{6b^2 a_1 + \delta_{fin}a_0}{4b^2\delta_{fin}}, \tag{24b}$$

and

$$a_{s+1} = \frac{2b^2(s+2)(s+1)a_s + \delta_{fin}s(s+1)a_{s-1} - (2s^2 - p)a_{s-2}}{b^2\delta_{fin}(s+3)(s+1)}, \quad s \geqslant 2. \tag{24c}$$

For $r_2 = 0$, the coefficients of the series

$$\theta_2(z) = \sum_{m=0}^{\infty}A_m z^m, \tag{25}$$

are

$$A_1 = 0, \tag{26a}$$

$$A_2 = -\frac{1}{2b^2}A_0, \tag{26b}$$

and

$$A_{s+1} = \frac{2b^2 s(s-1)A_s + \delta_{fin}(s-1)(s-2)A_{s-1} - [2(s-2)^2 - p]A_{s-2}}{b^2 \delta_{fin}(s+1)(s-1)}, \quad s \geqslant 2. \tag{26c}$$

Therefore, the general power series solution of ordinary differential Eq. (11) is

$$\begin{aligned}\theta(z) &= \sum_{m=0}^{\infty} a_m z^{m+2} + \sum_{m=0}^{\infty} A_m z^m \\ &= z^2(a_0 + a_1 z + a_2 z^2 + \cdots) + (A_0 + A_1 z + A_2 z^2 + \cdots)\end{aligned} \tag{27}$$

Since the coefficients of the series depend on the fin's geometrical parameters (b and δ_{fin}) as well as the dimensionless fin parameter p, the convergence of the series varies from case to case. The following power series convergence criterion can be used to ensure convergence for any fin case,

$$\lim_{m\to\infty} \left| \frac{a_{m+1} z^{m+3} + A_{m+1} z^{m+1}}{a_m z^{m+2} + A_m z^m} \right| < 1. \tag{28}$$

Eq. (27) is subject to the following boundary conditions that are of interest to micro-channel heat sink modeling.

2.2.1. Prescribed tip (x = 0) and base (x = b) temperatures

At $x = 0$ (or $z = b$),

$$\begin{aligned}\theta(b) &= \sum_{m=0}^{\infty} a_m b^{m+2} + \sum_{m=0}^{\infty} A_m b^m \\ &= b^2(a_0 + a_1 b + a_2 b^2 + \cdots) + (A_0 + A_1 b + A_2 b^2 + \cdots) \\ &= \theta_t.\end{aligned} \tag{29}$$

At $x = b$ (or $z = 0$),

$$\theta(0) = A_0 = \theta_b. \tag{30}$$

2.2.2. Prescribed tip temperature (x = 0) and adiabatic base (x = b)

At $x = 0$ (or $z = b$),

$$\begin{aligned}\theta(b) &= \sum_{m=0}^{\infty} a_m b^{m+2} + \sum_{m=0}^{\infty} A_m b^m \\ &= b^2(a_0 + a_1 b + a_2 b^2 + \cdots) + (A_0 + A_1 b + A_2 b^2 + \cdots) = \theta_t.\end{aligned} \tag{31}$$

At $x = b$ (or $z = 0$),

$$\begin{aligned}\left.\frac{d\theta}{dx}\right|_{x=b} &= -\frac{\sqrt{b^2 - z^2}}{z} \left.\frac{d\theta}{dz}\right|_{z=0} \\ &= -\frac{\sqrt{b^2 - z^2}}{z} \left[2\sum_{m=0}^{\infty} a_m z^{m+1} + \sum_{m=1}^{\infty} m a_m z^{m+1} + \sum_{m=1}^{\infty} m A_m z^{m-1} \right]\Bigg|_{z=0} \\ &= -(2ba_0 + 2bA_2) = 0.\end{aligned} \tag{32}$$

Combining Eq. (32) with Eq. (26b) yields

$$a_0 = \frac{1}{2b^2} A_0. \tag{33}$$

2.2.3. Adiabatic tip (x = 0) and prescribed base temperature (x = b)

At $x = 0$ (or $z = b$),

$$\begin{aligned}\left.\frac{d\theta}{dz}\right|_{z=b} &= \left[2\sum_{m=0}^{\infty} a_m z^{m+1} + \sum_{m=1}^{\infty} m a_m z^{m+1} + \sum_{m=1}^{\infty} m A_m z^{m-1} \right]\Bigg|_{z=b} \\ &= 2b(a_0 + a_1 b + a_2 b^2 + \cdots) + b^2(a_1 + 2a_2 b + 3a_3 b^2 + \cdots) \\ &\quad + (A_1 + 2A_2 b + 3A_3 b^2 + \cdots) = 0.\end{aligned} \tag{34}$$

At $x = b$ (or $z = 0$),

$$\theta(0) = A_0 = \theta_b. \tag{35}$$

The heat transfer rate at the fin base ($x = b$) is given by

$$\begin{aligned}q'_{fin} &= kA'_c \left.\frac{d\theta}{dx}\right|_{x=b} \\ &= -k\delta_{fin} \frac{\sqrt{b^2 - z^2}}{z} \left.\frac{d\theta}{dz}\right|_{z=0} \\ &= -k\delta_{fin} \frac{\sqrt{b^2 - z^2}}{z} \left[2\sum_{m=0}^{\infty} a_m z^{m+1} + \sum_{m=1}^{\infty} m a_m z^{m+1} + \sum_{m=1}^{\infty} m A_m z^{m-1} \right]\Bigg|_{z=0} \\ &= -k\delta_{fin} \Bigg[2\sqrt{b^2 - z^2}(a_0 + a_1 z + a_2 z^2 + \cdots) \\ &\quad + z\sqrt{b^2 - z^2}(a_1 + 2a_2 z + 3a_3 z^2 + \cdots) \\ &\quad + \frac{\sqrt{b^2 - z^2}}{z}(A_1 + 2A_2 z + 3A_3 z^2 + \cdots) \Bigg]\Bigg|_{z=0} = k\delta_{fin}(2ba_0 + 2bA_2).\end{aligned} \tag{36}$$

Notice that the right-hand-side terms of Eqs. (36) and (32) are proportional, which confirms that q'_{fin} has a zero value for the case of an adiabatic base.

3. Analytical model for heat sinks with circular micro-channels

To obtain analytical solutions for heat diffusion in the heat sinks shown in Fig. 1, the following assumptions are made based on the unit cells illustrated in Fig. 3:

1. In the case of one-sided heating, the top, right and left surfaces of the heat sink are insulated. In the case of two-sided heating, the horizontal mid-plane is adiabatic due to symmetry, and the right and left surfaces are insulated.
2. In the case of one-sided heating, Q_1 and Q_{2a} are averaged values over lower and upper quadrants of the wetted surface, respectively. These values are different for the case of one-sided heating.
3. The endwall width of the heat sink is equal to half the spacing between micro-channels, i.e., $W_{s,e} = 0.5W_s$.
4. Axial heat conduction effects in the micro-channel wall along the flow direction are neglected.

3.1. One-sided heating

As shown in Fig. 3(a), two separated quadrant regions must be considered for the analysis of a one-sided heated micro-channel heat sink. From the power series solution, the temperature distribution for the lower quadrant region can be written as

$$\begin{aligned}\theta(z) &= \sum_{m=0}^{\infty} a_m z^{m+2} + \sum_{m=0}^{\infty} A_m z^m \\ &= z^2(a_0 + a_1 z + a_2 z^2 + \cdots) + (A_0 + A_1 z + A_2 z^2 + \cdots)\end{aligned} \tag{37}$$

where

$$\hat{p} = \frac{hD}{k}, \tag{38}$$

$$z = \sqrt{0.25D^2 - x^2}, \tag{39}$$

$$a_1 = \frac{4}{3(W_s + D)} a_0, \tag{40a}$$

$$a_2 = \frac{1.5D^2 a_1 + (W_s + D)a_0}{D^2(W_s + D)}, \tag{40b}$$

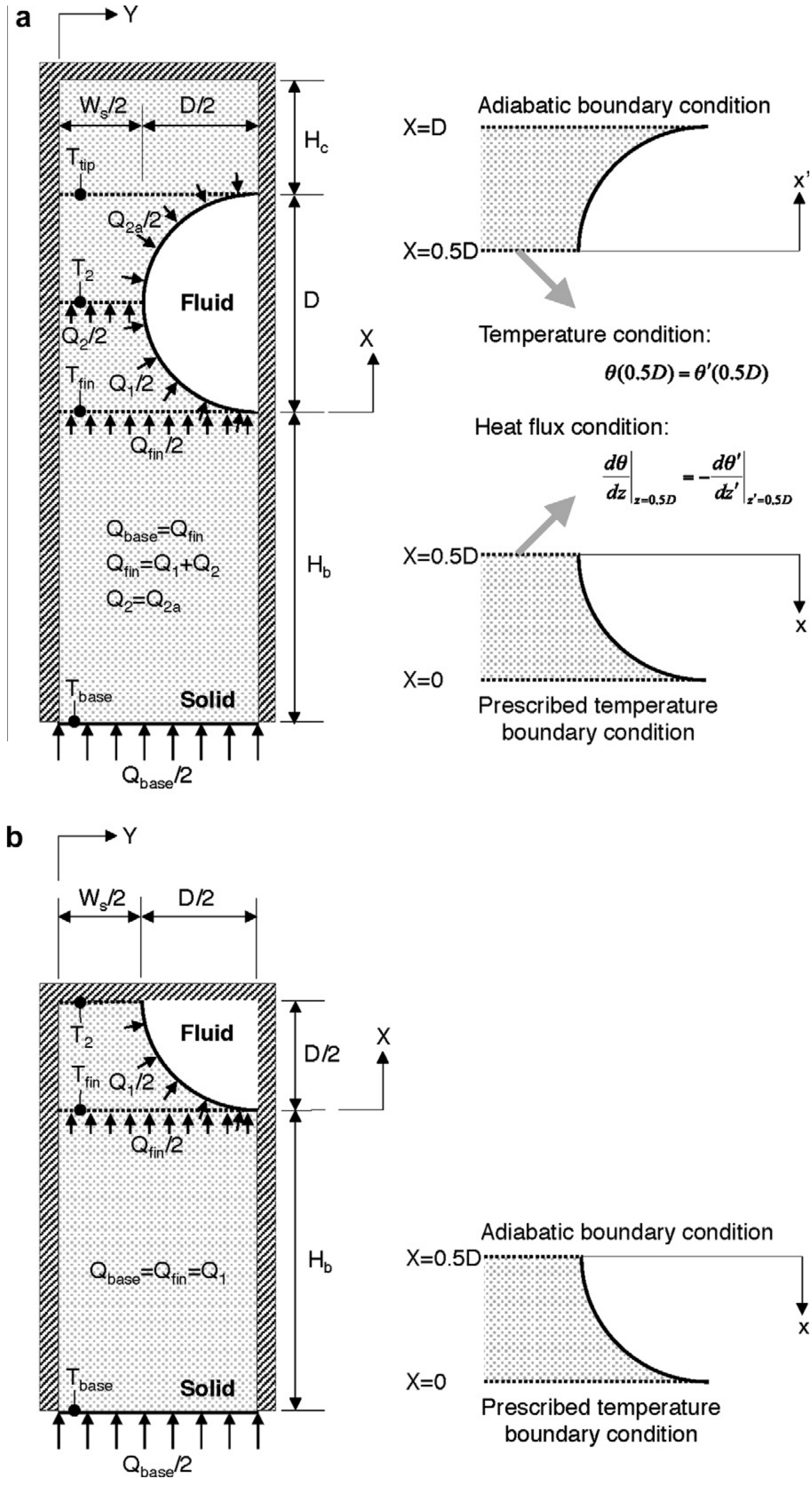

Fig. 3. Heat sink unit cells with (a) one-sided heating and (b) symmetrical two-sided heating.

$$a_{s+1} = \frac{0.5D^2(s+2)(s+1)a_s + (W_s+D)s(s+1)a_{s-1} - (2s^2-\hat{p})a_{s-2}}{0.25D^2(W_s+D)(s+3)(s+1)},$$
$$s \geqslant 2, \tag{40c}$$

$$A_1 = 0, \tag{41a}$$

$$A_2 = -\frac{2}{D^2}A_0, \tag{41b}$$

$$\text{and } A_{s+1}=\frac{0.5D^2s(s-1)A_s+(W_s+D)(s-1)(s-2)A_{s-1}-[2(s-2)^2-\hat{p}]A_{s-2}}{0.25D^2(W_s+D)(s+1)(s-1)},\quad s\geqslant 2. \tag{41c}$$

The temperature distribution for the upper quadrant region can be written as

$$\theta'(z')=\sum_{m=0}^{\infty}c_m z'^{m+2}+\sum_{m=0}^{\infty}C_m z'^{m} = z'^2(c_0+c_1z'+c_2z'^2+\cdots)+(C_0+C_1z'+C_2z'^2+\cdots) \tag{42}$$

where

$$z'=\sqrt{0.25D^2-x'^2}, \tag{43}$$

$$c_1=\frac{4}{3(W_s+D)}c_0, \tag{44a}$$

$$c_2=\frac{1.5D^2c_1+(W_s+D)c_0}{D^2(W_s+D)}, \tag{44b}$$

$$c_{s+1}=\frac{0.5D^2(s+2)(s+1)c_s+(W_s+D)s(s+1)c_{s-1}-(2s^2-\hat{p})c_{s-2}}{0.25D^2(W_s+D)(s+3)(s+1)},\quad s\geqslant 2, \tag{44c}$$

$$C_1=0, \tag{45a}$$

$$C_2=-\frac{2}{D^2}C_0, \tag{45b}$$

$$\text{and } C_{s+1}=\frac{0.5D^2s(s-1)C_s+(W_s+D)(s-1)(s-2)C_{s-1}-[2(s-2)^2-\hat{p}]C_{s-2}}{0.25D^2(W_s+D)(s+1)(s-1)},\quad s\geqslant 2. \tag{45c}$$

Since the coefficients $a_1,a_2,a_3,\ldots$, $A_1,A_2,A_3,\ldots$, $c_1,c_2,c_3,\ldots$, $C_1,C_2,C_3,\ldots$ are represented in terms of the primary coefficients a_0, A_0, c_0, C_0, respectively, only four boundary conditions are needed to solve Eqs. (37) and (42) as shown in Fig. 3(a). A prescribed temperature boundary is applied to the lower surface ($X = 0$) of the lower quadrant region. An adiabatic boundary condition is applied to top surface ($X = D$) of the upper quadrant region. The temperatures and heat fluxes are matched along the interface ($X = 0.5D$) between the upper and lower quadrant regions.

The following boundary conditions are applied to obtain the temperature distribution along $0 \leqslant X \leqslant D$.

3.1.1. Prescribed temperature at X = 0

At $x = 0.5\,D$ (or $z = 0$),

$$\theta(0)=A_0=\theta_b. \tag{46}$$

3.1.2. Adiabatic boundary at X = D

At $x' = 0.5D$ (or $z' = 0$),

$$\left.\frac{d\theta'}{dx'}\right|_{x'=0.5D}=-\frac{\sqrt{0.25D^2-z'^2}}{z'}\left.\frac{d\theta'}{dz'}\right|_{z'=0} =-\frac{\sqrt{0.25D^2-z'^2}}{z'}\left[2\sum_{m=0}^{\infty}c_m z'^{m+1}+\sum_{m=1}^{\infty}mc_m z'^{m+1}+\sum_{m=1}^{\infty}mC_m z'^{m-1}\right]\Bigg|_{z'=0}=-(Dc_0+DC_2)=0. \tag{47}$$

Combining Eqs. (47) and (45b) gives

$$c_0=\frac{2}{D^2}C_0. \tag{48}$$

3.1.3. Matching temperatures at X = 0.5D

At $x = x' = 0$ (or $z = z' = 0.5D$),

$$\theta(0.5D)=\theta'(0.5D). \tag{49}$$

$$0.25D^2(a_0+0.5Da_1+0.25D^2a_2+\cdots)+(A_0+0.5DA_1+0.25D^2A_2+\cdots) =0.25D^2(c_0+0.5Dc_1+0.25D^2c_2+\cdots)+(C_0+0.5DC_1+0.25D^2C_2+\cdots) \tag{50}$$

3.1.4. Matching heat fluxes at X = 0.5D

At $x = x' = 0$ (or $z = z' = 0.5D$),

$$\left.\frac{d\theta}{dz}\right|_{z=0.5D}=-\left.\frac{d\theta'}{dz'}\right|_{z'=0.5D}. \tag{51}$$

$$D(a_0+0.5Da_1+0.25D^2a_2+\cdots)+0.25D^2(a_1+Da_2+0.75D^2a_3+\cdots)+(A_1+DA_2+0.75D^2A_3+\cdots) =-[D(c_0+0.5Dc_1+0.25D^2c_2+\cdots)+0.25D^2(c_1+Dc_2+0.75D^2c_3+\cdots)+(C_1+DC_2+0.75D^2C_3+\cdots)] \tag{52}$$

The temperatures at the interface between the upper and lower quadrant regions (T_2 at $X = 0.5D$) and at the top surface of the upper quadrant region (T_{tip} at $X = D$) can be obtained from $\theta(0.5D) = \theta'(0.5D)$ and $\theta'(0)$, respectively.

Applying energy conservation to the lower quadrant region (see Fig. 3(a)) yields

$$Q_{base}=Q_{fin}=Q_1+Q_2[\mathrm{W/m}]. \tag{53}$$

From Eq. (36), the heat transfer rate at the fin base of the micro-channel unit cell can be written as

$$Q_{fin}=k(W_s+D)\left.\frac{d\theta}{dx}\right|_{x=0.5D}=kD(W_s+D)(a_0+A_2). \tag{54}$$

Applying an energy balance to the micro-channel heat sink shown in Fig. 1(a) yields

$$q''_{eff}A_{eff}=q''_{base}A_{base}=Q_{fin}LN, \tag{55}$$

where

$$A_{eff}=\pi DLN, \tag{56}$$

and

$$A_{base}=(W_s+D)LN. \tag{57}$$

3.2. Two-sided heating

Fig. 3(b) shows the mid-plane adiabatic boundary at $X = 0.5D$ created by the symmetry of two-sided heating. From the power series solution, the temperature distribution for $0 \leqslant X \leqslant 0.5D$ can be expressed as

$$\theta(z)=\sum_{m=0}^{\infty}a_m z^{m+2}+\sum_{m=0}^{\infty}A_m z^{m} = z^2(a_0+a_1z+a_2z^2+\cdots)+(A_0+A_1z+A_2z^2+\cdots) \tag{58}$$

where

$$z=\sqrt{0.25D^2-x^2}, \tag{59}$$

$$a_1=\frac{4}{3(W_s+D)}a_0, \tag{60a}$$

$$a_2=\frac{1.5D^2a_1+(W_s+D)a_0}{D^2(W_s+D)}, \tag{60b}$$

$$a_{s+1} = \frac{0.5D^2(s+2)(s+1)a_s + (W_s + D)s(s+1)a_{s-1} - [2s^2 - \hat{p}]a_{s-2}}{0.25D^2(W_s + D)(s+3)(s+1)},$$
$$s \geqslant 2, \tag{60c}$$

$$A_1 = 0, \tag{61a}$$

$$A_2 = -\frac{2}{D^2}A_0, \tag{61b}$$

and $$A_{s+1} = \frac{0.5D^2 s(s-1)A_s + (W_s + D)(s-1)(s-2)A_{s-1} - [2(s-2)^2 - \hat{p}]A_{s-2}}{0.25D^2(W_s + D)(s+1)(s-1)},$$
$$s \geqslant 2. \tag{61c}$$

The prescribed temperature and adiabatic boundary conditions are applied to the lower surface and the top surface of lower quadrant region, respectively.

3.2.1. Prescribed base temperature at X = 0

At $x = 0.5D$ (or $z = 0$),

$$\theta(0) = A_0 = \theta_b. \tag{62}$$

3.2.2. Adiabatic tip (at X = 0.5D)

At $x = 0$ (or $z = 0.5D$),

$$\left.\frac{d\theta}{dz}\right|_{z=0.5D} = \left[2\sum_{m=0}^{\infty} a_m z^{m+1} + \sum_{m=1}^{\infty} m a_m z^{m+1} + \sum_{m=1}^{\infty} m A_m z^{m-1}\right]\Bigg|_{z=0.5D}$$
$$= D(a_0 + 0.5Da_1 + 0.25D^2 a_2 + \cdots)$$
$$+ 0.25D^2(a_1 + Da_2 + 0.75D^2 a_3 + \cdots)$$
$$+ (A_1 + DA_2 + 0.75D^2 A_3 + \cdots) = 0. \tag{63}$$

Energy conservation for the lower quadrant region shown in Fig. 3(b) yields

$$Q_{base} = Q_{fin} = Q_1\,[\mathrm{W/m}]. \tag{64}$$

From Eq. (36), the heat transfer rate at the fin base of the micro-channel unit cell can be written as

$$Q_{fin} = k(W_s + D)\left.\frac{d\theta}{dx}\right|_{x=0.5D} = kD(W_s + D)(a_0 + A_2). \tag{65}$$

Applying an energy balance to the micro-channel heat sink shown in Fig. 1(b) yields

$$q''_{eff} A_{eff} = 2q''_{base} A_{base} = 2Q_{fin} LN, \tag{66}$$

where

$$A_{eff} = \pi DLN, \tag{67}$$

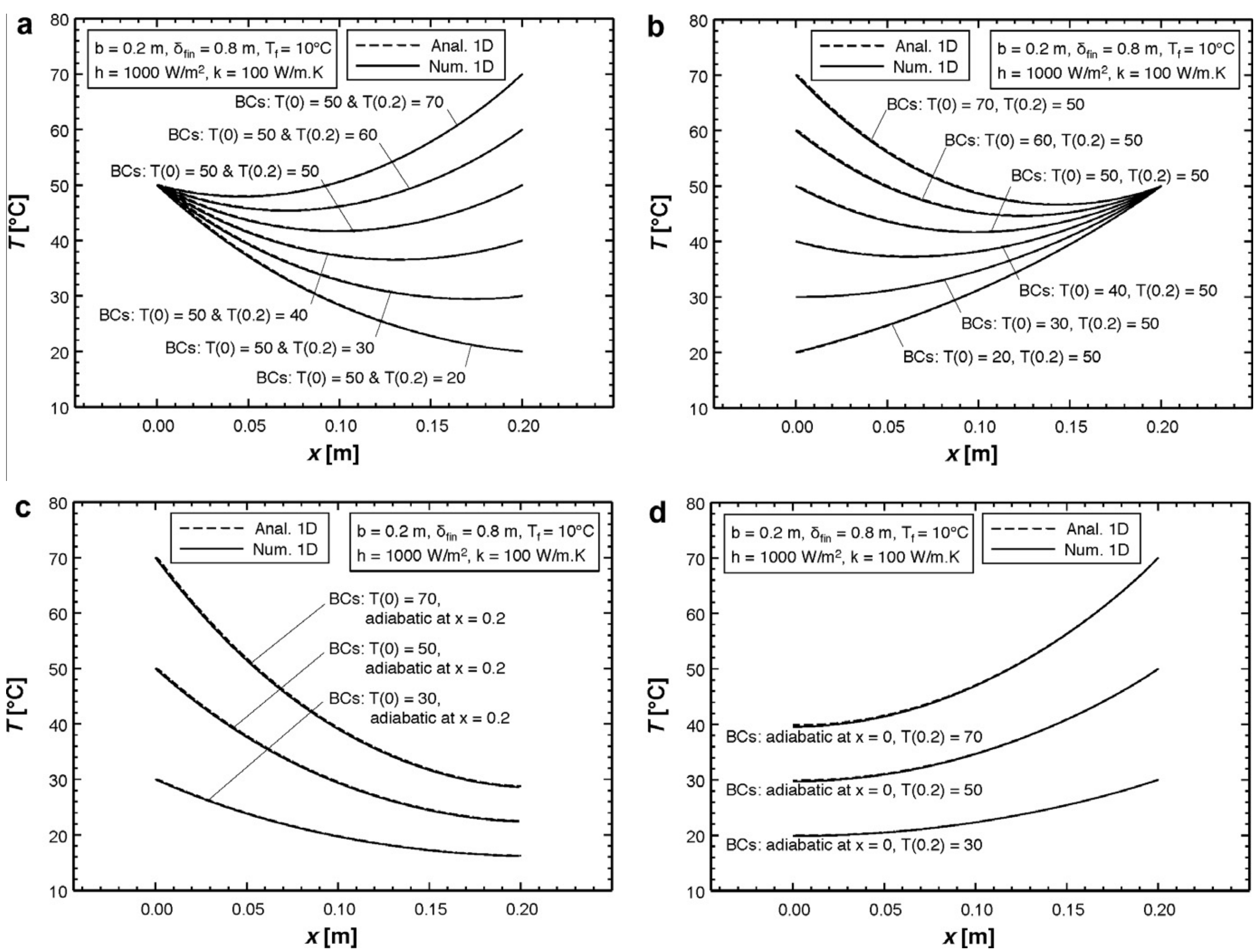

Fig. 4. Comparison of one-dimensional analytical and one-dimensional numerical results for longitudinal fin with circular profile with (a and b) prescribed tip and base temperatures, (c) prescribed tip temperature and adiabatic base, and (d) adiabatic tip and prescribed base temperature.

and

$$A_{base} = (W_s + D)LN. \tag{68}$$

4. Results

4.1. Validation of power series solution

To validate the present power series solutions, the one-dimensional analytical predictions are compared to one-dimensional numerical solutions of Eq. (5) for a longitudinal fin with a circular profile using MATLAB software [22]. Comparisons are made for four different sets of boundary conditions: prescribed tip temperature (50 °C) and base temperature (varied from 20 to 70 °C), Fig. 4(a), prescribed tip temperature (varied from 20 to 70 °C) and base temperature (50 °C), Fig. 4(b), prescribed tip temperature (30, 50, 70 °C) and adiabatic base, Fig. 4(c), and adiabatic tip and prescribed base temperature (30, 50, 70 °C), Fig. 4(d). All calculations were conducted using $b = 0.2$ m, $\delta_{\phi_{in}} = 0.8$ m, $T_f = 10$ °C, $h = 1{,}000$ W/m^2 K, and $k = 100$ W/m K. The power series with 20,000 terms was used to predict the temperature distribution; the effect of number of power series terms will be discussed later. It should be noted that, since Eq. (5) has a singularity at $x = b$, the numerical calculation excluded the singularity point. Fig. 4(a)–(d) shows that for all cases, the temperature distributions from the analytical solution are nearly identical to those from the one-dimensional numerical solution, which confirms the validity of the power series method.

Fig. 5 shows the dimensions examined in the present study for the cases of one-sided and two-sided heating surfaces. To examine the effects of micro-channel spacing and diameter, the dimensions of $D = 400$ μm with $W_s = 100$, 400 and 700 μm ($W_s/D = 0.25$, 1.00 and 1.75), Fig. 5(a), and $W_s = 86$ μm with $D = 124$, 326 and 528 μm ($W_s/D = 0.69$, 0.26 and 0.16), Fig. 5(b), are used. In the case of two-sided heating, symmetry yields an adiabatic boundary at $X = 0.5D$ as shown in Fig. 3(b), therefore only the domain below the plane at $X = 0.5D$ is used for calculating results for two-sided heating.

For validation of the analytical results, FLUENT 6.3 [23] was used to numerically solve the two-dimensional heat diffusion equation for each set of dimensions. All simulations were conducted based on copper as the heat sink solid using $k = 387.6$ W/m K, $h = 50{,}000$ W/m^2 K, $T_f = 300$ K, $q''_{base} = 300$ W/cm^2 (for one-sided heating) or $q''_{base} = 150$ W/cm^2 (for two-sided heating). A convergence criterion of 10^{-11} was applied to the residuals of the energy equation. The two-dimensional meshes were created using GAMBIT 2.2 software [24]. Grid independence was examined by using two grid systems with 71,000 and 213,000 cells, which resulted in temperature and heat transfer rate differences of less than 0.02%. For calculation efficiency, the grid system with 71,000 cells was used for all the simulations.

The temperature contours for one-sided heating and two-sided heating are shown in Figs. 6 and 7, respectively, for $D = 400$ μm with $W_s = 100$, 400 and 700 μm, and $W_s = 86$ μm with $D = 124$, 326 and 528 μm. For both cases, temperatures increase with increasing W_s/D. Because of symmetry, temperatures are more uniform around the coolant channel for two-sided heating than for one-sided heating. Notice that both cases display some departure from one-dimensional heat flow. For one-sided heating, Fig. 6(b) shows the temperature gradient in the Y-direction at $X = D$ increases with increasing diameter. For two-sided heating, Fig. 7(a) shows the temperature gradient in the Y-direction at $X = 0.5D$ increases with increasing spacing. A more systematic means for assessing the influence of W_s and D on the accuracy of the one-dimensional analytical power series solution will be discussed below.

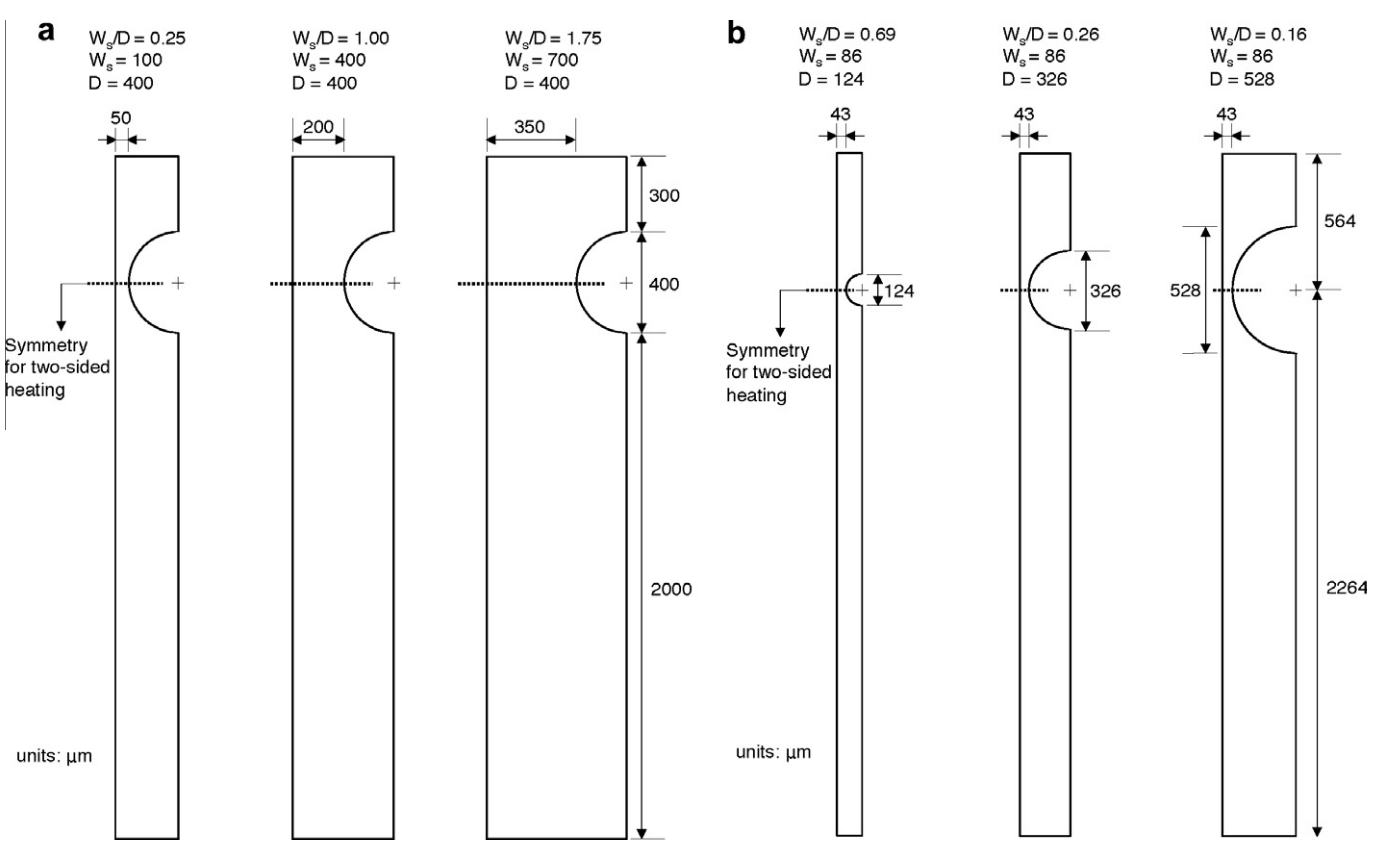

Fig. 5. Dimensions for one-sided heating case with (a) $D = 400$ μm with $W_s = 100$, 400 and 700 μm, and (b) $W_s = 86$ μm with $D = 124$, 326 and 528 μm.

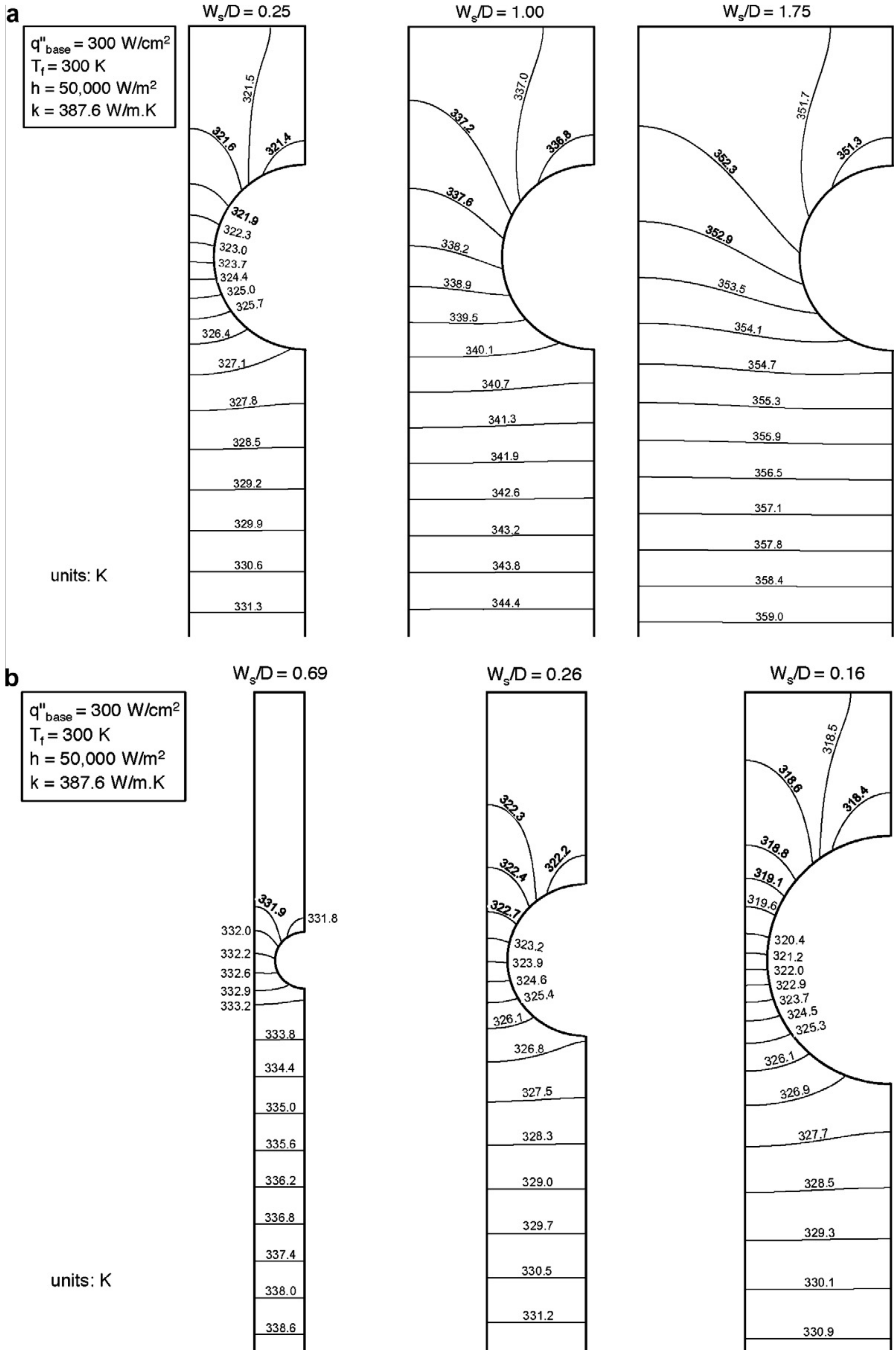

Fig. 6. Temperature contours for one-sided heating case with (a) D = 400 μm with W_s = 100, 400 and 700 μm, and (b) W_s = 86 μm with D = 124, 326 and 528 μm.

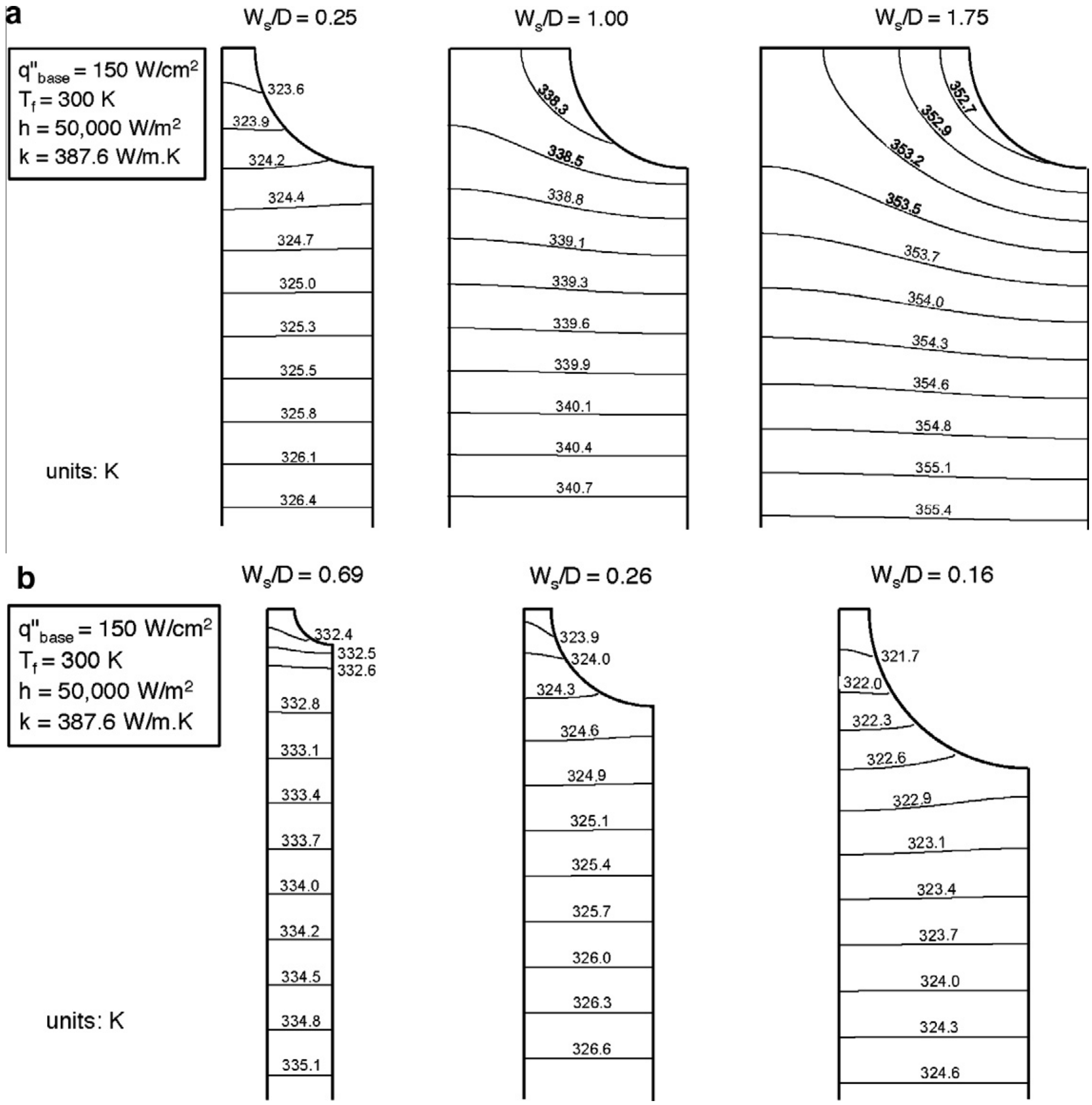

Fig. 7. Temperature contours for two-sided heating case with (a) D = 400 μm with W_s = 100, 400 and 700 μm, and (b) W_s = 86 μm with D = 124, 326 and 528 μm.

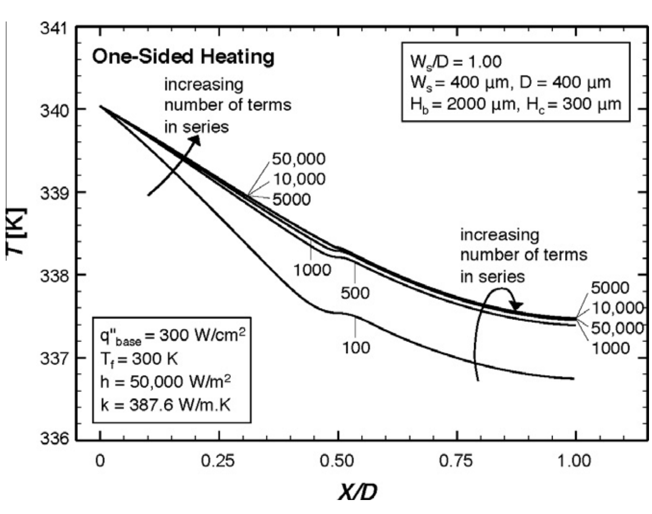

Fig. 8. Effects of number of terms in power series on solution convergence.

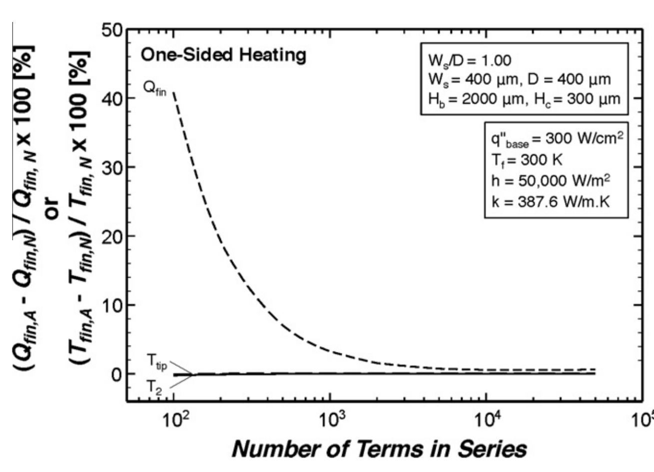

Fig. 9. Variation of percent difference between one-dimensional analytical and two-dimensional numerical (area-averaged) results with number of terms in power series for W_s/D = 1.00.

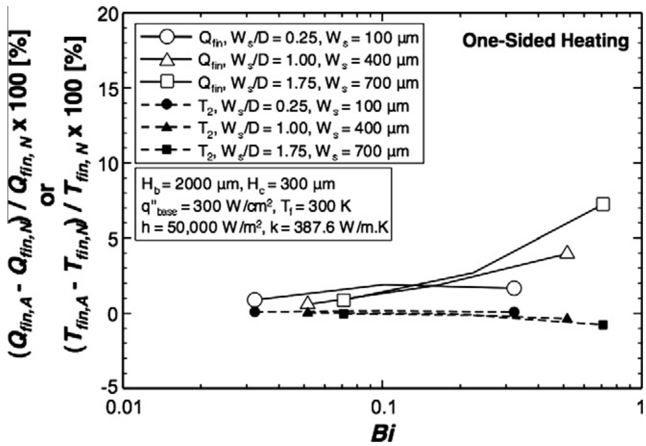

Fig. 10. Variation of percent difference between one-dimensional analytical and two-dimensional numerical (area-averaged) results with Biot number for W_s/D = 0.25, 1.00, and 1.75.

4.2. Effects of number of terms of power series solution

Fig. 8 shows the one-dimensional temperature distribution for the case of W_s = 400 μm and D = 400 μm as predicted by the power series solution. Temperature predictions are plotted for different number of terms used in the series. An infinite number of terms would ensure converge to the exact solution. However, Fig. 8 shows temperature distributions after 10,000 terms are nearly identical, which is why 20,000 terms were used earlier in all the analytical solutions.

Fig. 9 shows the variation of percent differences in Q_{fin}, T_2, and T_{tip} between the two-dimensional numerical results (FLUENT results) and present analytical solutions with number of terms in the series. It shows that a relatively small number of terms is needed to accurately predict the values of T_2 (0.2% with 100 terms), T_{tip} (0.1% with 100 terms) and Q_{fin} (1.6% with 2000 terms) compared to the temperature distribution within the X/D domain.

4.3. Effects of Biot number

Fig. 10 shows the percent differences in Q_{fin} and T_2 between the two-dimensional (area-averaged) numerical results and analytical solutions for one-sided heating with W_s/D = 0.25, 1.00 and 1.75, and Bi ranging from 0.03 to 0.71. Overall, the percent difference in Q_{fin} increases with increasing Bi, with higher W_s/D values yielding higher Q_{fin} differences. Nonetheless, these differences become significant only for high Bi values that are beyond the range of interest for practical electronic cooling applications. Fig. 10 shows the percent difference in T_2 is fairly insensitive to Bi or W_s/D.

4.4. Effects of micro-channel spacing and diameter: one-sided heating

The temperature distributions for one-sided heating are shown in Fig. 11 for W_s/D = 0.25, 1.00 and 1.75, and Fig. 12 for W_s/D = 0.69, 0.26 and 0.16. The input values of $q''_{base} = 300\,\mathrm{W/cm^2}$, h = 50,000 W/m² K, T_f = 300 K and k = 387.6 W/m K were used for the one-dimensional analytical and two-dimensional numerical calculations. The two-dimensional numerical results shown correspond

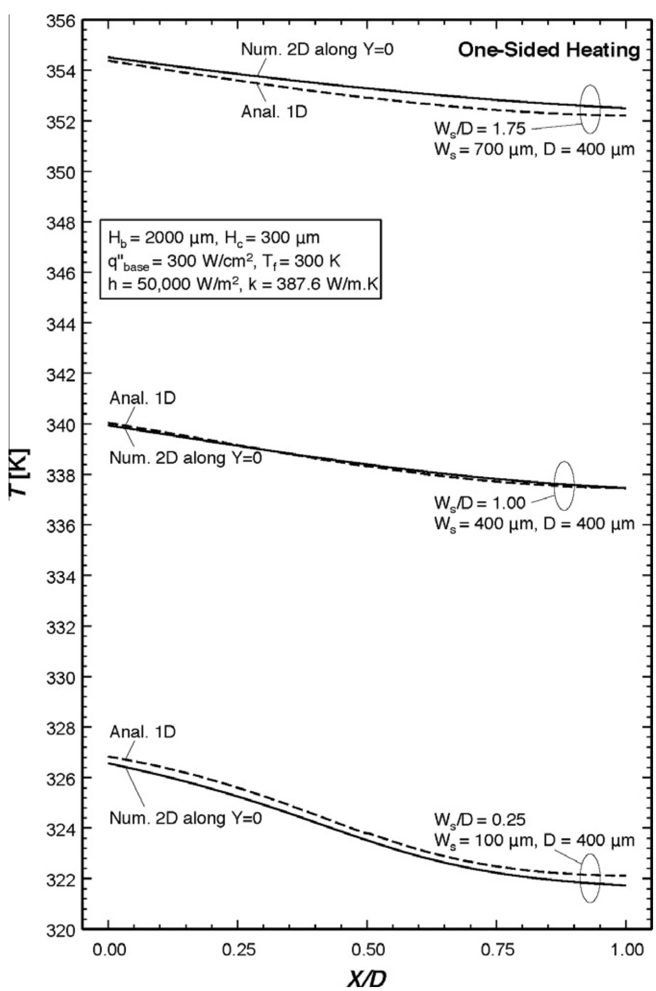

Fig. 11. Temperature distributions for one-sided heating with W_s/D = 0.25, 1.00 and 1.75.

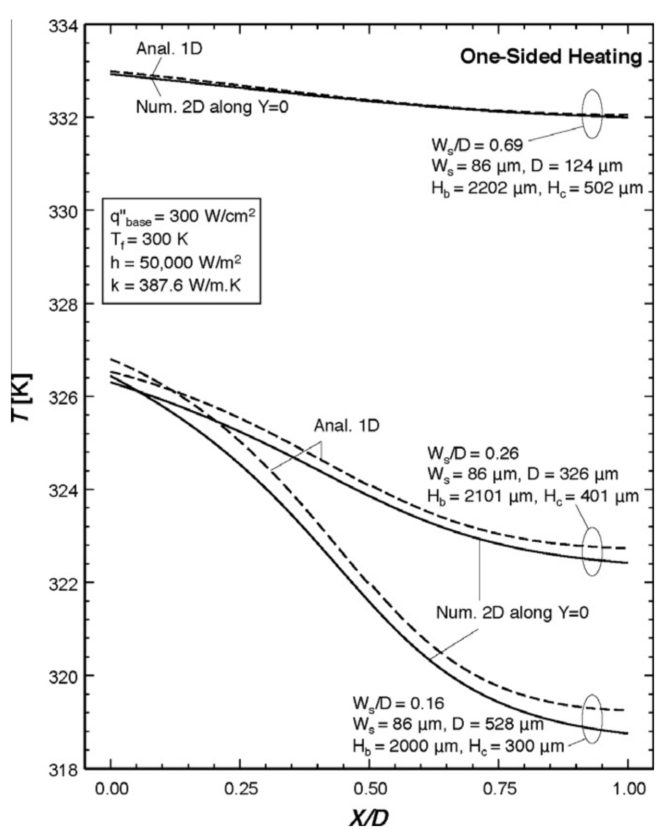

Fig. 12. Temperature distributions for one-sided heating with W_s/D = 0.69, 0.26 and 0.16.

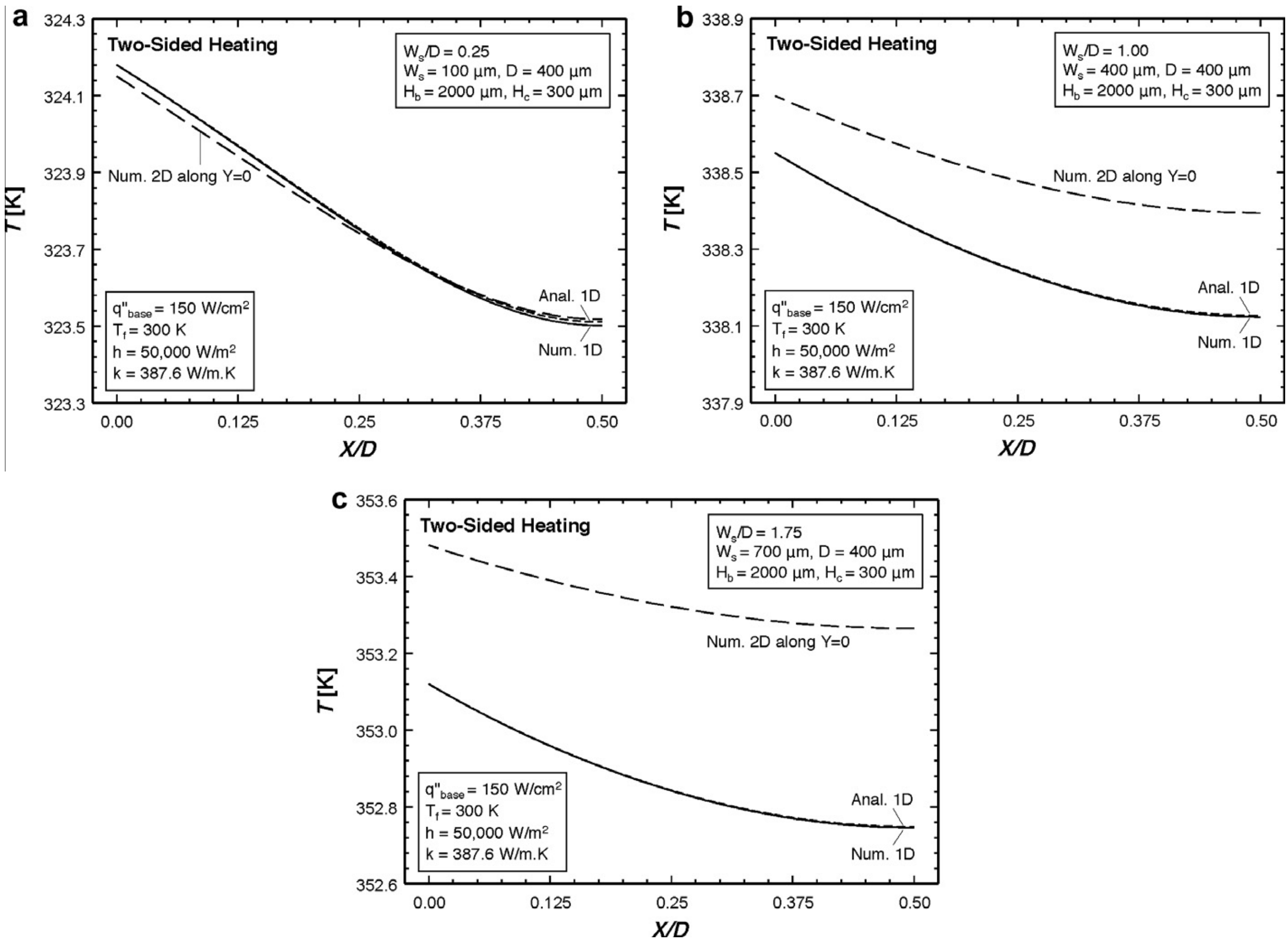

Fig. 13. Temperature distributions for two-sided heating with W_s/D = 0.25, 1.00 and 1.75.

to $Y = 0$ (see Fig. 3). Because of relatively weak Y-direction temperature gradients, Figs. 11 and 12 show the present analytical model predictions are nearly identical to those of the two-dimensional numerical results corresponding to $Y = 0$. Fig. 11 shows that for a fixed diameter of $D = 400$ μm, the mean temperature for $0 < X/D < 1$ decreases with decreasing channel spacing, W_s. Fig. 12 shows that for a fixed spacing of $W_s = 86$ μm, the mean temperature for $0 < X/D < 1$ decreases with increasing diameter, D. Moreover, the temperature difference between $X = 0$ and $X = D$ increases with increasing channel diameter, D, because of the increased heating perimeter. Therefore, a micro-channel with small channel spacing and large channel diameter (i.e., with small value of W_s/D) provides a better thermal performance.

4.5. Effects of micro-channel spacing and diameter: two-sided heating

The temperature distributions for two-sided heating are shown in Fig. 13 for W_s/D = 0.25, 1.00 and 1.75, and Fig. 14 for W_s/D = 0.69, 0.26 and 0.16. The input values of $q''_{base} = 150\,\mathrm{W/cm^2}$, h = 50,000 W/m^2 K, T_f = 300 K and k = 387.6 W/m K were used for the one-dimensional analytical, one-dimensional numerical and two-dimensional numerical calculations. Figs. 13 and 14 show that the temperature distributions from one-dimensional analytical solutions are nearly identical to those from the one-dimensional numerical solutions, and very close to those from the two-dimensional numerical simulations. Similar to one-sided heating, a heat sink with a small value of W_s/D shows better thermal performance.

Comparing Figs. 11–13 and Figs. 12–14 shows that the temperature differences for two-sided heating along X/D are much smaller than those for one-sided heating.

4.6. Assessment of overall accuracy of analytical models

To assess the accuracy of the analytical models for realistic heat sink geometries, values of percent differences in the temperatures and the heat transfer rates for $D = 400$ μm with W_s = 100, 400 and 700 μm, and $W_s = 86$ μm with D = 124, 326 and 528 μm, with Bi ranging from 0.014 to 0.071, are provided in Table 1. Overall, the percent differences for two-sided heating are smaller than those for one-sided heating. Very good agreement is realized between the present analytical model predictions and the two-dimensional numerical simulations, with maximum differences in temperature and heat transfer rate of 0.23% and 1.33%, respectively.

5. Conclusions

This study examined heat diffusion effects in micro-channel heat sinks containing arrays of circular micro-channels. A new one-dimensional analytical solution technique was presented to predict the temperature distribution in heat sinks subjected to one-sided and two-sided heating. The analytical results were compared to one-dimensional and two-dimensional numerical simulations for different micro-channel diameters, spacings, and Biot

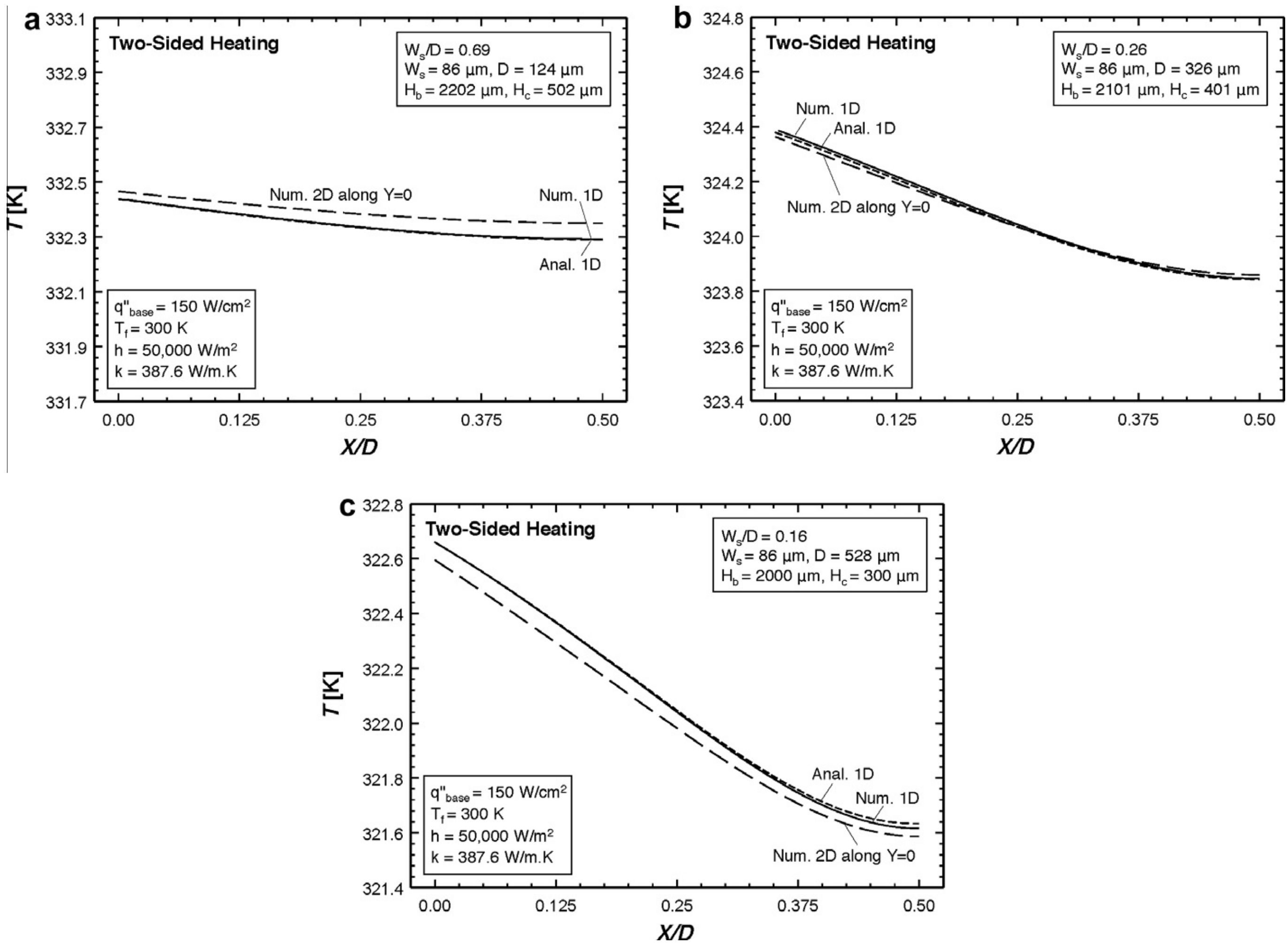

Fig. 14. Temperature distributions for two-sided heating with W_s/D = 0.69, 0.26 and 0.16.

Table 1
Comparison of two-dimensional numerical (area-averaged) and one-dimensional analytical results.

	Units	Num.	Anal.	%Diff.	Num.	Anal.	%Diff.	Num.	Anal.	%Diff.
One-sided heating										
D = 400 μm		W_s = 100 μm (*Bi* = 0.032)			W_s = 400 μm (*Bi* = 0.052)			W_s = 700 μm (*Bi* = 0.071)		
T_{base}	K	342.32	–		355.52	–		369.85	–	
T_{fin}	K	326.84	326.84	0.00	340.04	340.04	0.00	354.38	354.37	0.00
T_2	K	323.50	323.80	0.09	338.27	338.32	0.02	353.01	352.91	−0.03
T_{tip}	K	321.52	322.12	0.18	337.06	337.46	0.12	351.88	352.20	0.09
$Q_{fin} = Q_{base}$	W/m	1500.0	1513.3	0.89	2400.0	2414.1	0.59	3300.0	3329.0	0.88
W_s = 86 μm		D = 124 μm (*Bi* = 0.014)			D = 326 μm (*Bi* = 0.027)			D = 528 μm (*Bi* = 0.040)		
T_{base}	K	350.03	–		342.79	–		342.28	–	
T_{fin}	K	332.99	332.99	0.00	326.53	326.53	0.00	326.80	326.80	0.00
T_2	K	332.33	332.37	0.01	323.84	324.10	0.08	321.57	321.99	0.13
T_{tip}	K	331.90	332.06	0.05	322.24	322.74	0.15	318.52	319.25	0.23
$Q_{fin} = Q_{base}$	W/m	630.0	632.0	0.32	1236.0	1245.3	0.75	1842.0	1866.8	1.33
Two-sided heating										
D = 400 μm		W_s = 100 μm (*Bi* = 0.032)			W_s = 400 μm (*Bi* = 0.052)			W_s = 700 μm (*Bi* = 0.071)		
T_{base}	K	331.92	–		346.29	–		360.86	–	
T_{fin}	K	324.18	324.18	0.00	338.55	338.55	0.00	353.12	353.12	0.00
T_2	K	323.49	323.51	0.01	338.27	338.13	−0.04	353.00	352.75	−0.07
$Q_{fin} = Q_{base}$	W/m	750.00	747.51	−0.33	1200.0	1200.8	0.07	1650.0	1659.3	0.56
W_s = 86 μm		D = 124 μm (*Bi* = 0.014)			D = 326 μm (*Bi* = 0.027)			D = 528 μm (*Bi* = 0.040)		
T_{base}	K	340.96	–		332.51	–		330.40	–	
T_{fin}	K	332.44	332.44	0.00	324.39	324.38	0.00	322.66	322.66	0.00
T_2	K	332.33	332.29	–0.01	323.84	323.84	0.00	321.57	321.63	0.02
$Q_{fin} = Q_{base}$	W/m	315.00	315.58	0.18	618.00	615.96	–0.33	921.00	918.00	–0.33

%Diff. = (it $T_A - T_N)/T_N \times 100$ [%] or $(Q_A - Q_N)/Q_N \times 100$ [%].

numbers. Key findings from the study can be summarized as follows:

(1) Because of a singularity point, the governing second-order ordinary differential equation for one-dimensional steady-state temperature distribution in the heat sink has no exact solution. An alternative analytical power series solution technique is presented in which the differential equation is recast in polynomial form. This technique is shown to yield very accurate predictions for both longitudinal fins with circular profiles and heat sinks containing circular micro-channels.
(2) Predictions of the power series solution are validated for different heat sink channel diameters and spacings, and both one-sided and two-sided heating conditions using one-dimensional numerical two-dimensional numerical simulations. Superior cooling performance is achieved by decreasing spacing-to-diameter ratio.
(3) Overall, maximum percent differences in temperature and heat transfer rate between the analytical and two-dimensional numerical results of 0.23% and 1.33%, respectively, prove the present analytical models are very accurate and effective tools for the design and thermal resistance prediction of micro-channel heat sinks found in electronic cooling applications.

Acknowledgement

The authors are grateful for the support of the Office of Naval Research (ONR) for this study.

References

[1] K.A. Triplett, S.M. Ghiaasiaan, S.I. Abdel-Khalik, A. LeMouel, B.N. McCord, Gas-liquid two-phase flow in micro-channels Part II: void fraction and pressure drop, Int. J. Multiphase Flow 25 (1999) 395–410.
[2] L. Jiang, M. Wong, Y. Zohar, Forced convection boiling in a micro-channel heat sink, J. Microelectromechanical Syst. 10 (2001) 80–87.
[3] W. Qu, I. Mudawar, Flow boiling heat transfer in two-phase micro-channel heat sinks-I. Experimental investigation and assessment of correlation methods, Int. J. Heat Mass Transfer 46 (2003) 2755–2771.
[4] J. Lee, I. Mudawar, Two-phase flow in high-heat-flux micro-channel heat sink for refrigeration cooling applications: Part II - heat transfer characteristics, Int. J. Heat Mass Transfer 48 (2005) 941–955.
[5] I. Tiselj, G. Hetsroni, B. Mavko, A. Mosyak, E. Pogrebnyak, Z. Segal, Effect of axial conduction on the heat transfer in micro-channels, Int. J. Heat Mass Transfer 47 (2004) 2551–2565.
[6] G. Liu, J. Xu, Y. Yang, W. Zhang, Active control of flow and heat transfer in silicon micro-channels, J. Micromech. Microeng. 20 (2010) 045006.
[7] W. Qu, G.M. Mala, D. Li, Heat transfer for water flow in trapezoidal silicon micro-channels, Int. J. Heat Mass Transfer 43 (2000) 3925–3936.
[8] A. Megahed, I. Hassan, Two-phase pressure drop and flow visualization of FC-72 in a silicon micro-channel heat sink, Int. J. Heat Fluid Flow 30 (2009) 1171–1182.
[9] H. Wu, X. Wu, Z. Wei, Flow friction and heat transfer of ethanol-water solutions through silicon micro-channels, J. Micromech. Microeng. 19 (2009) 045005.
[10] A. Husain, K.Y. Kim, Thermal optimization of a micro-channel heat sink with trapezoidal cross section, J. Electron. Packag. 131 (2009) 021005.
[11] R.L. Webb, M. Zhang, Heat transfer and friction in small diameter channels, Microscale Thermophys. Eng. 2 (1998) 189–202.
[12] C.P. Tso, S.P. Mahulikar, Experimental verification of the role of Brinkman number in micro-channels using local parameters, Int. J. Heat Mass Transfer 43 (2000) 1837–1849.
[13] I. Mudawar, M.A. El-Masri, C.S. Wu, J.R. Ausman-Mudawar, Boiling heat transfer and critical heat flux in high-speed rotating liquid films, Int. J. Heat Mass Transfer 28 (1985) 795–806.
[14] M.B. Bowers, I. Mudawar, High flux boiling in low flow rate, low pressure drop mini-channel and micro-channel heat sinks, Int. J. Heat Mass Transfer 37 (1994) 321–332.
[15] I. Mudawar, M.B. Bowers, Ultra-high critical heat flux (CHF) for subcooled water flow boiling - I. CHF data and parametric effects for small diameter tubes, Int. J. Heat Mass Transfer 42 (1999) 1405–1428.
[16] D.D. Hall, I. Mudawar, Ultra-high critical heat flux (CHF) for subcooled water flow boiling - II. High-CHF database and design parameters, Int. J. Heat Mass Transfer 42 (1999) 1429–1456.
[17] S.M. Kim, I. Mudawar, Analytical heat diffusion models for different micro-channel heat sink cross-sectional geometries, Int. J. Heat Mass Transfer 53 (2010) 4002–4016.
[18] W.M. Murray, Heat dissipation through an annular disk or fin of uniform thickness, J. Appl. Mech. 60 (1938) A-78.
[19] K.A. Gardner, Efficiency of extended surface, Trans. ASME 67 (1945) 621–631.
[20] F.P. Incropera, D.P. Dewitt, Fundamentals of Heat and Mass Transfer, 5th ed., Wiley, New York, NY, 2002.
[21] A.D. Polyanin, V.F. Zaitsev, Handbook of Exact Solutions for Ordinary Differential Equations, CRC, Boca Raton, FL, 1995.
[22] The Mathworks Inc., Matlab R2009a user's guide, Natick, MA (2009).
[23] FLUENT Inc., Fluent 6 user's manual, Lebanon, NH (2006).
[24] FLUENT Inc., Gambit 2 user's manual, Lebanon, NH (2006).